Desalination and Water Treatment
www.deswater.com
doi: 10.5004/dwt.2018.23000

133 (2018) 177–190
November

Removal of phosphate from aqueous solutions using modified activated carbon prepared from agricultural waste (*Populous caspica*): optimization, kinetic, isotherm, and thermodynamic studies

Zeinab Gholami[a], Seid Kamal Ghadiri[b], Moayed Avazpour[c,d], Mohammad Alizadeh Fard[e], Nader Yousefi[a], Seyedeh Solmaz Talebi[f], Mohammad Khazaei[g], Mohammad Hossien Saghi[h], Amir Hossein Mahvi[a,i,j,*]

[a]*Department of Environmental Health Engineering, School of Public Health, Tehran University of Medical Sciences, Tehran, Iran, emails: ahmahvi@yahoo.com (A.H. Mahvi), Zeinab.gholami_tums@yahoo.com (Z. Gholami)*
[b]*Department of Environmental Health Engineering, School of Public Health, Shahroud University of Medical Sciences, Shahroud, Iran, email: Kamalgh2005@gmail.com*
[c]*Department of Environmental Health Engineering, School of Public Health, Shahid Beheshti University of Medical Sciences, Tehran, Iran, email: m_f_1859@yahoo.com*
[d]*Department of Environmental Health Engineering, Ilam University of Medical Science, Ilam, Iran*
[e]*Michigan Technological University, Houghton, MI, United States, email: malizade@mtu.edu*
[f]*Department of Epidemiology, School of Public Health, Shahroud University of Medical Sciences, Shahroud, Iran, email: Talebi_solmaz@yahoo.com*
[g]*Department of Environmental Health Engineering, School of Public Health, Hamadan University of Medical Sciences, Hamadan, Iran, email: khazaei57@gmail.com*
[h]*Department of Environmental Health Engineering, School of Public Health, Sabzevar University of Medical Sciences, Sabzevar, Iran, email: mohamadsaghi@gmail.com*
[i]*Center for Solid Waste Research (CSWR), Institute for Environmental Research (IER), Tehran University of Medical Sciences (TUMS), Tehran, Iran*
[j]*National Institute of Health Research, Tehran University of Medical Sciences, Tehran, Iran*

Received 8 March 2018; Accepted 25 August 2018

ABSTRACT

Activated carbon was successfully prepared from *Populous caspica* wood by a thermochemical reduction method and modified by grafting amine groups. In the batch tests, pH, initial phosphate concentration, reaction time, and adsorbent dose were evaluated to remove phosphate (PO_4^{3-}) from the aqueous phase. The response surface method was chosen to study the composition effect of independent input factors and one dependent output response (removal efficiency). The *p*-value (2.2×10^{-16}), *F*-value (116.6), R^2 (multiple: 0.9774, adjusted: 0.97), and lack of fit (0.167) indicated that the reduced quadratic model is highly significant for the phosphate removal using aminated activated carbon. The maximum efficiency removal of phosphate (92.76%) was obtained at pH, initial phosphate concentrations, contact time, and adsorbent dose of 3, 10 mg L^{-1}, 60 min, and 90 mg L^{-1}, respectively. The adsorption data fitted well with the Freundlich isotherm and pseudo-second-order kinetic model. Therefore, the intraparticle diffusion was the dominant adsorption mechanism but it was not the sole rate controlling step. In addition, regeneration process with five repetitions of regeneration cycles showed high desorption efficiencies and slight loss of spent adsorbent initial adsorption capacity. Thus, the results recommended that modified activated carbon prepared from agricultural waste (*P. caspica*) could properly remove phosphate from aqueous solution.

Keywords: Agricultural waste; Amination; Phosphate; Optimization; Kinetic; Isotherm

* Corresponding author.

1. Introduction

Phosphate has been produced in many industries such as fertilizers, detergents, water softeners, and food product industries [1]. This anion has been widely entered to the water bodies due to human activities, deposition of minerals, or rock mines through natural processes, decomposition of cleaning products and discharge of industrial wastewater [2]. Phosphorus is often present at low concentrations in the wastewater mostly as phosphates including organic phosphate, inorganic phosphate, oligophosphates, and polyphosphate [3]. Phosphorus, such as nitrogen, is one of the key nutrients that cause eutrophication in the aquatic environments [4]. High phosphate concentration in aquatic environments is leading to the growth of photosynthetic algae and cyanobacteria [5]. Eutrophication phenomenon needs 0.005–0.05 mg L^{-1} phosphate concentration [6]. Phosphate concentration in water usually is 0.2 mg L^{-1} [7] and the effluent standard for discharge to surface waters is 6 mg L^{-1} [8]. The various treatment techniques have been employed for the removal of phosphate from water and wastewater [9] such as chemical precipitation [10], ion exchange [11], nanofiltration [12], electrocoagulation [13], biological treatment [14], and adsorption methods [15]. Most physical methods such as membrane technologies are expensive and the rate of phosphate removal with biological methods is low [16]. Chemical methods are often required as a complementary process for the other methods. Chemical precipitation with iron, alum, lime, and magnesium is the most common methods for removing phosphate from wastewater [17]. Flocculation is known as a good method for removing phosphate, but the removal efficiency is not high at low phosphate concentration and also much sludge is formed [18].

Ion exchange process is considered as an inexpensive method for treating organic and inorganic contaminants. Among all ion exchange methods, grafting amine groups (GAG) modification process onto the carbon-based material to produce weak base anion exchangers has been used for the removal of various contaminants such as anions from aqueous solutions [19,20].

One of the most interesting forms of carbon is graphene-like reduced carbon sheets. These sheets have a high capacity to absorb metal cations due to their high specific surface area (2,200–3,300 m^2 g^{-1}) and abundant hydroxide and carboxylic groups on their surfaces [21,22]. Studies on the possibility of attracting fluoride, perchlorate, dyes such as methylene blue, methyl violet, Rhodamine B, and Orange G have been taken on the graphene nanosheet [23–26]. Populous tree wood was used as a base carbon for this study because of high growth rate and production of high-quality wood, poplar trees have a good potential for wood cultivation. This kind of trees in Iran is densely planted for growing wood and application such as lumber, palate, pulp, paper, and biofuels. The aim of this study was to synthesize particular graphene-like reducing black carbon sheets recovered from wood waste of populous tree (widely grown across North America, Europe, and Asia) modification of black carbon by GAG method and phosphate removal efficiency from aqueous solutions. These days, application of agro-wastes as good adsorbents has been studied in pollutants removal from water and wastewater [27–31]. The response surface method (RSM) is considered a good statistical method which interaction between variables and responses determined [32]. In addition, RSM could be determined the optimizations between variables. Also, the central composite design (CCD) as a method of RSM, resulted in significantly better models, having more levels (five levels) and designing experimental data according to the rotatable mode which gives more accurate models comparing with the other methods [33]. According to the CCD, the interaction between the independent variables (initial phosphate concentration, pH, time contact, and adsorbent dose) and dependent response variable (phosphate removal efficiency) is simultaneously considered and optimization process was carried out based on the interaction between all independent variables and effect of them on the response variable.

Therefore, CCD was used for experimental design and optimization of variables on the adsorption of phosphate onto graphene-like reduced carbon sheets (RGC).

2. Materials and methods

2.1. Preparation of graphene-like reduced carbon sheets

In this study, *Populous caspica* shaving wood was used as the main raw material for a production of graphene-like RGC. First, shaving woods were dried in the air under the sunlight over 10 d. Then, 10 kg of dried shaving woods were burned under local weather conditions and turned into black carbon in an open field. After cooling, the impurities of wood black carbon (WBC) were separated by laboratory mesh (<177 μm) and thermochemically reduced according to our previous work [19]. Briefly, after sonication for 1 h and filtration of samples, 10 g of dry WBC were treated with KOH/WBC ratio of 10 in 1,000 mL of deionized water for removal of impurities and penetration of KOH into carbon layers. Following filtration, washing thoroughly with deionized water to neutral pH, drying and crashing, the residues were further activated in nitrogen gas flow at 800°C to obtain graphene-like RGC from *P. caspica* shaving wood.

2.2. Surface modification of RGC recovered by the amine groups

10 g of RGC recovered was added to the 120 mL of dimethylformamide (*N*, *N*-dimethylformamide). Then, 100 mL of Epichlorohydrin was increased to the mixture and stirred for 1 h at 100°C. In addition, 40 mL catalyst Pyridine was added to the mixture and again stirred for 1 h at 100°C. The product was rinsed with 2 L of diluted ethanol solution (ethanol: water = 1:1) at 40°C to remove excess Pyridine and Epichlorohydrin precipitates. Next, 100 mL of dimethylamine solution (50%) was added to the mixture, and the final mixture was stirred for 3 h at 100°C. Finally, the resultant product was washed with 2 L of ethanol solution (50%), 2 L of 0.1 M NaOH solution, and 2 L of 0.1 M HCl solution.

2.3. Phosphate adsorption experiments

Adsorption studies were done with the following procedure. Synthetic solutions of phosphate were obtained from KH_2PO_4 (Merck, Germany). A stock solution of 1,000 mg L^{-1} of 99.5% KH_2PO_4 was prepared to make phosphate standard solutions with different concentrations (1–9 mg L^{-1}). Adsorption on carbon plates was carried out in a batch state using 250 mL erlens. The effects of independent and

effective variables on the adsorption process including pH (3–11), initial phosphate concentrations (10–90 mg L^{-1}), contact time (15–60 min), and adsorbent dose (10–90 mg L^{-1}) were evaluated at room temperature (24°C ± 2°C). According to the four variables mentioned above, the number of 38 runs was determined using *R* software (RSM). Phosphate concentration in the samples was determined with the UV spectrophotometer screening method according to the standard method at 516 nm. Obtained adsorbent materials were subjected to characterize using X-ray fluorescence (XRF), Fourier-transform infrared spectroscopy (FTIR), and scanning electron microscopy (SEM). Statistical analysis was also performed using *R* software.

2.4. Experimental design with RSM

RSM is an efficient statistical tool that has been employed in the statistical design of experiments, data analysis, and optimization of the operating conditions by considering the interactions between variables. In this study, numbers of experiments were carried out using CCD for predicting and modeling complicated relations between input-independent factors (pH (X_1), initial phosphate concentration (X_2), reaction time (X_3), and adsorbent dose (X_4)) and dependent factor (phosphate removal efficiency(Y)) under the optimum operational conditions. The actual values of the independent variables that were used for the experimental design are tabulated in Table 1.

Each independent variable which its range was determined ranges based on a set of preliminary experiments, was varied at three levels as –1, 0, and 1, respectively. The experimental design was conducted on *R* software for Windows (version 3.0.3:6 March 2014). The total number of experiments conducted for the four factors determined according to Eq. (1).

$$\text{Number of experiments} = 2^k + 2k + 15 \tag{1}$$

where k is the number of input variables. Consequently, 38 runs were designed using a 16 full factorial (the base design), 8 axial points, and 15 replicates in the center point.

A quadratic model as Eq. (2) was used to express the interaction between (Y) and (X_1, X_2, X_3, and X_4):

$$\gamma = B_0 + \sum_{i=1}^{k} B_i X_i + \sum_{i=1}^{k} B_{ii} X_i^2 + \sum_{i=1}^{k-1} \sum_{j=1}^{k} B_{ij} X_i X_j + C \tag{2}$$

Table 1
Coded values of independent variables used for experimental design

		Coded level		
Variable		–1	0	1
		Values		
pH	x_1	3	7	11
Initial phosphate concentration (mg L^{-1})	x_2	10	50	90
Time (min)	x_3	15	37.5	60
Adsorbent dose (mg L^{-1})	x_4	10	50	90

where B_0 is the intercept value, B_i, B_{ii}, and B_{ij} refer to the regression coefficient for linear, second order, and interactive effects, respectively. X_i and X_j are the independent variables, and C denotes the error of prediction [34].

2.5. Adsorption isotherms and kinetics

The relationship between the equilibrium amount of adsorbate that adsorbed onto the adsorbent (RGC) and the amount of remaining adsorbate on the solution was expressed through adsorption isotherm. It is an important step in the design of adsorption systems [35]. The experimental data for phosphate removal were fitted with adsorption models (Langmuir, Freundlich, and Temkin). The Langmuir original Eq. (3) and its linear form (4) are expressed as follow:

$$q_e = \frac{q_m b C_e}{1 + b C_e} \tag{3}$$

$$\frac{C_e}{q_e} = \frac{C_e}{q_m} + \frac{1}{q_m b} \tag{4}$$

where q_e is the equilibrium capacity of adsorbate (mg g^{-1}), C_e is the equilibrium concentration of adsorbate (mg L^{-1}), q_m the is maximum adsorption capacity (mg g^{-1}), and b is the Langmuir constant (L mg^{-1}).

The Freundlich original equation and its linear form are expressed as follows:

$$q_e = K_f C_e^{1/n} \tag{5}$$

$$\log(q_e) = \log K_f + \frac{1}{n} \log C_e \tag{6}$$

where q_e is the amount of adsorbate (mg g^{-1}), C_e is the equilibrium concentration of adsorbate (mg L^{-1}), and K_f (L g^{-1}) and $1/n$ (dimensionless) are the Freundlich constants.

The Temkin equation is expressed as follow:

$$q_e = B_1 \ln(K_t) + B_1 \ln(C_e) \tag{7}$$

where K_t is the equilibrium binding constant (L mg^{-1}) and B is the variation of adsorption energy (KJ mol^{-1}). K_t and B can be calculated from the slope and intercept of the linear plot of q_e (mg g^{-1}) versus ln C_e (mg L^{-1}).

The kinetics of phosphate adsorption onto the RGC was studied with pseudo-first-order and pseudo-second-order kinetic models. Pseudo-first-order defined by the following equation:

$$\frac{dq_t}{dt} = k_1 (q_e - q_t) \tag{8}$$

where q_e and q_t (mg g^{-1}) are the amount of phosphate adsorbed at equilibrium conditions and at time t (min), respectively. The rate constant of the pseudo-first-order kinetic model is k_1 (min^{-1}). The linear form of the pseudo-first-order as follows:

$$\log(q_e - q_t) = \log q_e - \left(\frac{k_1}{2.303} t \right) \tag{9}$$

Pseudo-second-order equation is as follows:

$$\frac{dq_t}{dt} = k_2\left(q_e - q_t\right)^2 \tag{10}$$

where k_2 is the rate constant (g mg^{-1} min). The linear forms of the pseudo-first-order as follows:

$$\frac{t}{q_e} = \frac{t}{k_2 q_e^2} + \frac{t}{q_e} \tag{11}$$

where the value of k_2 and q_e can be determined from the slope and intercept of the plot t/q_t versus t, respectively.

2.6. Thermodynamic study

The thermodynamic study was carried out at various temperatures (288K, 298K, and 308K). The main factors in thermodynamic study standard Gibbs free energy ($\Delta G°$), standard entropy ($\Delta S°$), and standard enthalpy ($\Delta H°$). ΔG is estimated based on the following equations:

$$\Delta G = -RT\ln K_0 \tag{12}$$

and

$$\Delta G = \Delta H - T\Delta S \tag{13}$$

where R is the universal gas constant (8.314 J mol^{-1} K), T and K_0 represent the temperature of solution (K) the equilibrium constant, respectively. In addition, standard entropy ($\Delta S°$) and standard enthalpy ($\Delta H°$) is obtained from the slope and intercept of the plot ln K_0 versus $1/T$, respectively.

2.7. Desorption and regeneration study

The spent aminated RGC obtained from the optimum experiments was regenerated with eluting HCl (0.1 mol L^{-1}) solution. In this step, the exhausted aminated RGC was agitated in solution/solid ratio of 50:1 for 1 h and 220 rpm. Then, the desorbed phosphate concentration of the supernatant was analyzed after solid phase separation with centrifuge equipment at 15,000 rpm for 3 min also, the regenerated aminated RGC was twice washed with deionized water and used as the phosphate adsorbent for the next cycles. Similar adsorption–regeneration procedures were carried out five times.

3. Results and discussion

3.1. Adsorbent characteristics

Physical and chemical properties of the WBC were determined by XRF, SEM, and FTIR. The chemical composition of adsorbent, which was conducted by XRF, is shown in Table 2. The main chemical components of WBC were alumina (11.03%) and silicon dioxide (15.53%).

Field emission scanning electron microscopy (FESEM) provides topographical and elemental information with a virtually unlimited depth of field. The FESEM images of the aminated RGC before (a) and after (c) phosphate uptake are shown in Fig. 1. While the surface of the adsorbent showed irregular texture with fine particles size, rough surface, and leaf-like edges. This structure can efficiently increase adsorption area. Particles with the thickness of less than 20 nm were detected (Fig. 1(a)). The EDS spectra of the aminated RGC, before (b) and after (d) phosphate uptake are presented in Fig. 1 to investigate its localized elemental information. O, C, Ca, Mg, Fe, and Al are the elements throughout the surface of aminated RGC with weight percentages of 40%, 29.25%, 2.1%, 1.8%, and 0.3%, respectively. So that, it indicates that phosphate was added to the elements after the adsorption (Fig. 1(d)).

Table 2
Chemical composition of natural used adsorbent (w/w)

Component	(w/w%)
Magnesium oxide (MgO)	4.84
Alumina (Al_2O_3)	11.03
Silicon dioxide (SiO_2)	15.53
Phosphorus pentoxide (P_2O_5)	4.17
Sulfur trioxide (SO_3)	2.13
Potassium oxide (K_2O)	4.38
Calcium oxide (CaO)	6.59
Scandium oxide (Sc_2O_3)	0.61
Titanium dioxide (TiO_2)	0.21
Manganese (II) oxide (MnO)	0.15
Iron (III) oxide (Fe_2O_3)	7.17
Strontium oxide (SrO)	0.82
Zinc oxide (ZnO)	0.24
Barium oxide (BaO)	0.13
Loss on ignition	40.78

FTIR image of the aminated RGC at wavelengths in the range 400–4,000 cm^{-1} for before (2(a)) and after (2(b)) of phosphate uptake is shown in Fig. 2. The adsorption band at ~1,799 cm^{-1} was assigned to carbonyl groups due to the symmetric stretching vibration of C=O. The intense broad peak at ~1,415 cm^{-1} represented the bending vibration of the C–H band. The peaks at ~1,048 cm^{-1} can be allocated to alcohols groups due to the symmetric stretching vibration of C–O band. Furthermore, the small peak at ~1,000 cm^{-1} can be assigned to C–N band or regional vibration of reductive carbon in the crystal lattice [36–38].

3.2. Quadratic models for adsorption of phosphate onto the aminated RGC adsorbent

To investigate the individual and combined effects of variables on the phosphate removal efficiency, adsorption experiments were conducted on the specified combinations of the effective parameters. CCD design matrix was employed to evaluate the contribution of four influential factors including pH, initial phosphate concentration, time, and adsorbent dose. The experimental design of 38 runs with the experimental and predicted data for the removal of phosphate by aminated RGC adsorbent in the CCD experimental design is presented in Table 3. It can be seen that the adsorption capacities vary intensely in order to the values

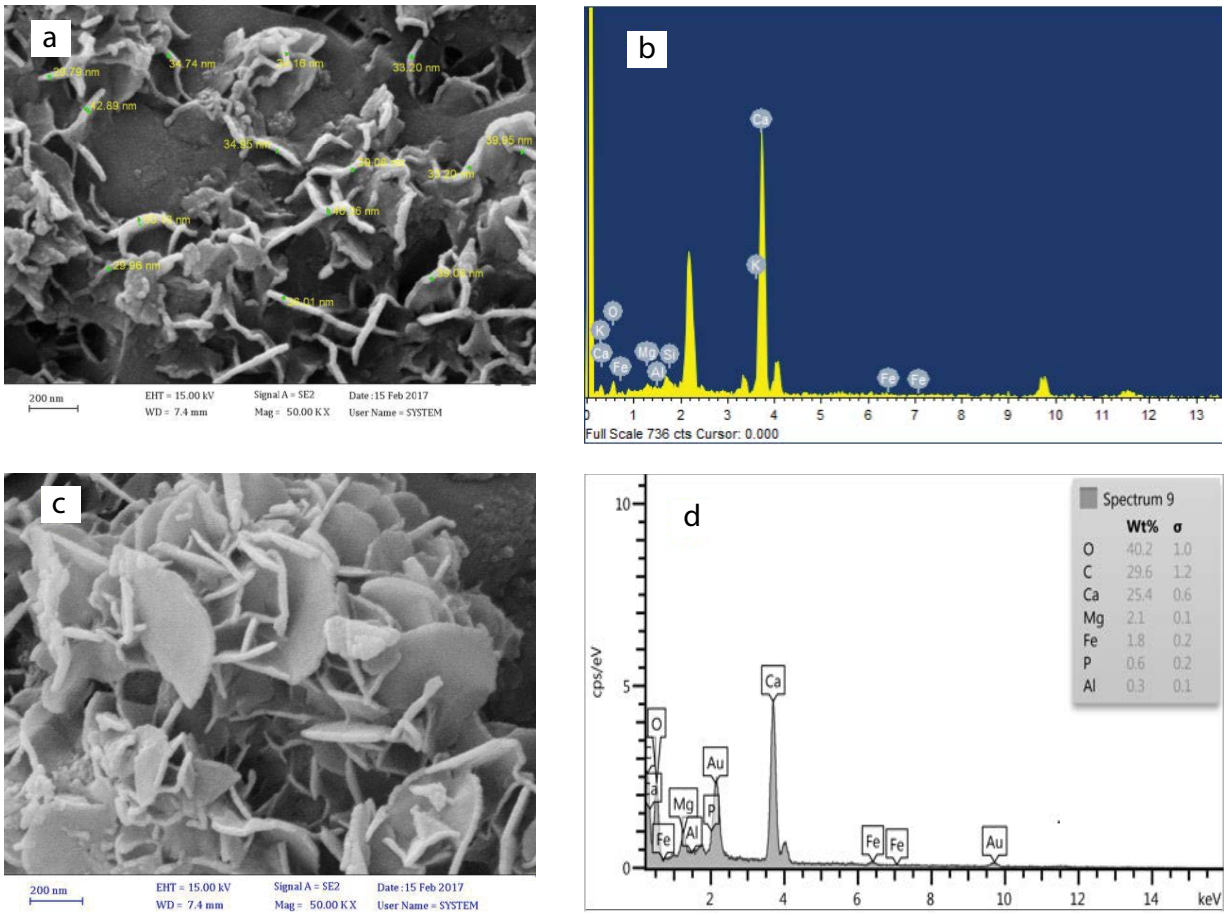

Fig. 1. FE-SEM image and EDS spectrum of aminated RGC before (a, b), and after (c, d) phosphate adsorption.

of the effective factors. To identify the optimum conditions, the RSM results need to be studied through the optimization process. Therefore, it has been suggested that the results in Table 3 can be used to determine optimum conditions. In addition, according to Table 3, it clears that phosphate removal efficiencies are between 10.12% (run 2) and 92.76% (run 21). Moreover, the lowest phosphate removal efficiency was observed in the run numbers 2, 5, 8, 10, 11, 18, and 30 that would be probably due to higher pH level and/or lower adsorbent concentration. When low adsorbent concentration and high pH level were combined (e.g., run 2) the antagonistic effect was very significant and the phosphate removal efficiency decreased significantly.

According to the results tabulated in Table 3, the time had no significant effect on the phosphate adsorption onto aminated RGC (run numbers of 2, 5, and 18), run 21 had obviously the optimum condition, as it showed the highest removal efficiency, and also the pH was a very important parameter in this case. However, the pH and adsorbent dosage were suitable to be deliberated as optimum conditions, as can be seen in runs 4, 6, and 31. The pH at acidic condition may cause serious operational difficulties in water treatment processes. Therefore, economically the operational conditions for run 31 with pH 7, initial phosphate concentration of 5 mg L^{-1}, time of 37.5 min, and adsorbent dosage of 9 g L^{-1} are the better runs.

3.3. Development of regression model equation and model analysis

The reduced quadratic model was generated by multiple regression analysis on the experimental data which is summarized in Table 4. According to Table 4, the pH (X_1), initial phosphate concentration (X_2), time (X_3), and adsorbent dosage (X_4) are significant (p-values < 0.05). Therefore, all parameters in Table 4 could influence model formulation. It can be seen that time (X_3), adsorbent dosage (X_4), X_1: X_2, X_2: X_3, and X_3^2 have a synergistic effect on the response prediction by the model, while pH (X_1), initial phosphate concentration (X_2), X_1: X_4, X_1^2, and X_4^2 have an antagonistic effect.

Phosphate removal efficiency predicted by the model is presented in Table 3. There is a linear correlation between the response predicted by the model and experimental data obtained in the laboratory. This shows the reliability of the model. The equations of quadratic model, for both coded and not coded, values of the parameters are shown in Eqs. (14) and (15), respectively. Therefore, these models can be used for prediction and optimization.

$$\gamma Po_4^{-3} = 3.123548 + 22.084456X_1 - 4.567439X_2 - 0.857177X_3 + 9.727948X_4 + 0.317383X_1X_2 - 0.129805X_1X_4 + 0.031535X_2X_3 - 1.847668X_1^2 + 0.010484X_3^2 - 0.387043X_4^2 \quad (14)$$

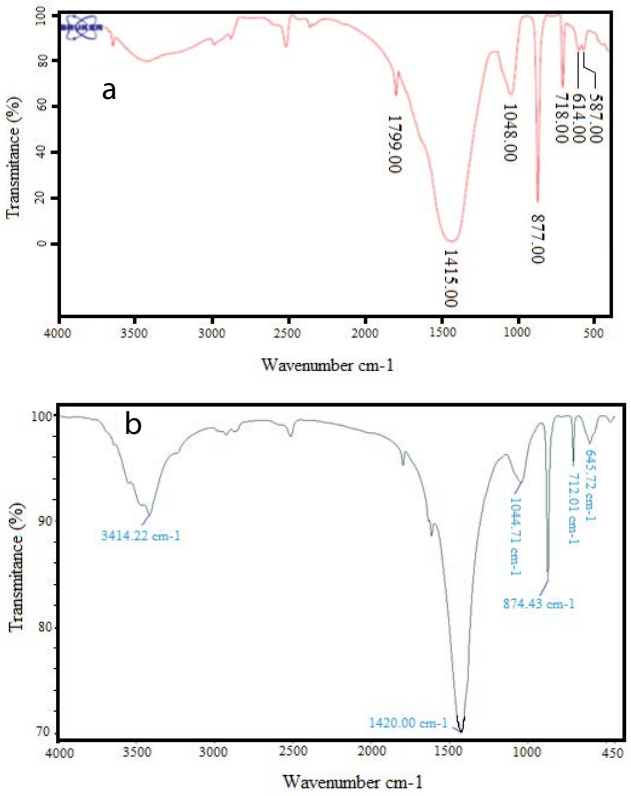

Fig. 2. T-IR spectra of aminated RGC before (a), and after (b) phosphate adsorption.

$$\gamma Po_4^{-3} = 78.38189 - 11.38X_1 - 4.65283X_2 + 1.95222X_3 + 19.79556X_4 + 5.07813X_1X_2 - 2.07688X_1X_4 + 2.83813X_2X_3 - 29.56268X_1^2 + 5.30732X_3^2 - 6.19268X_4^2 \quad (15)$$

The model adequacy can be described by ANOVA analysis, R^2 and adjusted R^2 are shown in Table 5. The ANOVA analysis is a statistical technique that statistical significance and accuracy of the models can be recognized via high F,

Table 4
Regression analysis for the reduced quadratic model

Model term	Coefficient estimate	Std. error	t-Value	p-Value
Intercept	78.38189	0.94766	82.7106	2.2×10^{-16}
X_1	–11.38000	0.96077	–11.8447	3.341×10^{-12}
X_2	–4.65283	0.99019	–4.6989	6.841×10^{-05}
X_3	1.95222	0.96077	2.0319	0.052106
X_4	19.79556	0.96077	20.6039	2.2×10^{-16}
$X_1 : X_2$	5.07813	1.01905	4.9832	3.186×10^{-05}
$X_1 : X_4$	–2.07688	1.01905	–2.0381	0.051450
$X_2 : X_3$	2.83813	1.01905	2.7851	0.009663
X_1^2	–29.56268	2.40116	–12.3118	1.377×10^{-12}
X_3^2	5.30732	2.40116	2.2103	0.035745
X_4^2	–6.19268	2.40116	–2.5790	0.015676

Table 3
CCD experimental design for phosphate removal by aminated RGC adsorbent

Run	Independent factors				Expt.	Pred.	Run	Independent factors				Expt.	Pred.
	X_1	X_2	X_3	X_4	Removal (%)	Removal (%)		X_1	X_2	X_3	X_4	Removal (%)	Removal (%)
1	3	1	15	1	44.43	48.06	20	7	5	37.5	5	76.68	78.38
2	11	1	60	1	10.12	17.52	21	3	1	60	9	92.76	90.03
3	7	5	37.5	5	83.17	78.38	22	7	5	37.5	5	76.12	78.38
4	7	5	37.5	5	84.66	78.38	23	7	5	37.5	5	76.42	78.38
5	11	9	60	1	20.92	24.05	24	3	9	60	9	73.88	76.24
6	7	5	37.5	5	84.08	78.38	25	7	5	37.5	5	73.97	78.38
7	11	9	15	9	45.32	49.90	26	7	5	37.5	5	76.28	78.38
8	11	9	15	1	18.11	14.47	27	7	5	37.5	5	80.77	78.38
9	7	5	37.5	5	81.64	78.38	28	7	5	37.5	5	82.37	78.38
10	3	9	15	1	20.07	22.92	29	7	5	37.5	5	76.53	78.38
11	7	5	37.5	5	25.41	19.29	30	11	5	37.5	5	38.18	37.44
12	3	1	15	9	90.08	91.80	31	7	5	37.5	9	89.54	91.98
13	3	9	15	9	70.43	66.66	32	7	5	37.5	5	76.72	78.38
14	3	1	60	1	50.92	46.28	33	7	1	37.5	5	82.97	83.03
15	11	9	60	9	63.18	59.48	34	3	5	37.5	5	56.21	60.20
16	7	5	37.5	5	76.71	78.38	35	7	5	15	5	81.77	81.73
17	11	1	15	9	53.97	54.73	36	7	5	60	5	82.36	85.64
18	3	9	60	1	35.93	32.50	37	7	5	37.5	1	51.59	52.39
19	11	1	15	9	54.66	52.96	38	7	5	37.5	5	76.17	78.38

X_1: pH, X_2: Initial Phosphate concentration (mg L^{-1}), X_3: Time (min), X_4: adsorbent dosage (g L^{-1}).

Table 5
Analysis of variance (ANOVA) for the reduced quadratic mode

Model formula in RSM X_1, X_2, X_3, X_4	DF	Sum of squares	Mean square	F-value	Probability (p)
First-order response	4	9,967.2	2,491.79	149.9697	2.2×10^{-16}
TWI (x_1, x_2)	1	412.6	412.60	24.8324	3.186×10^{-5}
TWI (x_1, x_4)	1	69.0	69.01	4.1537	0.051450
TWI (x_2, x_3)	1	128.9	128.88	7.7567	0.009663
Pure quadratic response	3	8,797.4	2,932.44	176.4923	2.2×10^{-16}
Residuals	27	448.6	16.62		
Lack of fit	13	274.8	21.14	1.7031	0.167540
Pure error	14	173.8	12.14		

Notes: Multiple R-squared: 0.9774, Adjusted R-squared: 0.97, F-statistic: 116.6 on 10 and 27 DF, p-value: < 2.2×10^{-16}.

low p-value, correlation coefficient (R), and lack of fit. Also, p-value less than 0.05 demonstrates the model terms are significant and the values greater than 0.10 imply they are not significant. The lack of fit value indicates the variation of response around the fitted model; this parameter should be insignificant if the model fits data well. According to the ANOVA analysis in Table 5, the higher F-value of 116.6 with a p-value lower than 0.0001 implies that the second-order polynomial model is statistically significant, thus the model fitted well with the experimental results. The F-values of linear and quadratic terms of the model are 149.96 and 176.49, which demonstrated the model and the individual coefficients of the model were more significant. The lack of fit value of the model (0.167) showed the significant correlation between factors and phosphate removal as a response (Table 5). In general, the efficiency of the model was described by R^2 value, however, the multiple R-squared value (0.977) closes to one and was very close to the adjusted R-squared value (0.97) which presented a satisfactory adjustment between quadratic model and experimental data [39].

3.4. Response surface methodology and contour plotting

In order to investigate the effects of different parameters and their interactions on the efficiency of phosphate adsorption onto aminated RGC adsorbent, the contour plots are presented based on the model coefficients in Figs. 3(a)–(f). It is distinguished that in these plots the effect of two variables was studied. The effect of phosphate concentration and pH solution on the removal efficiency at the time of 37.5 min and adsorbent dosage of 50 mg L^{-1} is shown in Fig. 3(a). The removal percentage of phosphate changed by varying the phosphate concentration and pH value. According to the results, at pH range of 6.5–7, with increasing in phosphate concentration from 10 to 45, the removal efficiency decreased from 85% to 80%, keeping the adsorbent dosage constant at 50 mg L^{-1} and the contact time at 37.5 min; in other words, removal efficiency decreased by increasing or/and decreasing pH. This fact showed that pH plays an important role in the adsorption process. The pH variations can control both the adsorption condition and also precipitation of materials [40]. Fig. 3(b) shows the effects of time and pH in the removal efficiency of phosphate by aminated RGC adsorbent. The pH range of 6.5–7, with increasing contact time from 45 to 60 min, and keeping the phosphate concentration constant at 48.9 mg L^{-1} and adsorbent dosage at 50 mg L^{-1}; removal efficiencies increased from 80% to 85%. The interacting effects of adsorbent dosage (X_4) and pH (X_1) are shown in Fig. 3(c). At a constant phosphate concentration of 48.9 mg L^{-1} and 37.5 min of reaction time, the phosphate removal efficiency improved from 60% to 90% with increasing the adsorbent dose from 10 to 80 mg L^{-1}. It indicated that adsorbent dosage is a significant factor in improving removal efficiency. This can be allocated to contact surfaces of the sorbent and more available adsorption sites, the diffusion of the phosphate into the adsorbent, and also increase the accessible active sites on the adsorbent. The maximum phosphate removal was obtained for adsorbent doses higher than 80 mg L^{-1} and the pH of 6.5. Based on the results presented in Fig. 3(d), at pH of 7 and the adsorbent dose of 50 mg L^{-1}, removal efficiency increased from 76% to 86% with decreasing initial phosphate concentration from 90 to 10 mg L^{-1}, and increasing contact time from 20 to 60 min, respectively. In Fig. 3(e), the effects of adsorbent dose and initial phosphate concentration are shown at pH of 7 and contact time of 37.5 min. When adsorbent dosage increased from 10 to 90 mg L^{-1} and phosphate concentration decreased from 90 to 10 mg L^{-1}, the removal efficiency increased from 50% to 95%. As shown in Fig. 3(f), the efficiency of phosphate removal increased from 55% to 95% with an increase of the adsorbent dosage to 90 mg L^{-1}, and the contact time to 60 min. According to the results, it is clear that the adsorbent dose and pH were the most effective variables in the phosphate removal efficiency.

3.5. Process optimization and model validity

The Solver "Add-ins" in Microsoft Excel was employed to achieve the optimum adsorption condition through the model equation predicted by RSM. These parameters involved pH (3–11), initial phosphate concentration (10–90 mg L^{-1}), contact time (5–60 min), and the adsorbent dosage (10–90 mg L^{-1}). In the optimum conditions, all parameters simultaneously were desirable criteria, and in the predicted optimal conditions the maximum removal efficiency was estimated to be 100%. The predicted optimal conditions by the Solver "Add-ins" were pH of 5.74, initial phosphate concentration of 10 mg L^{-1}, and contact time of 32.5 min and adsorbent dosage of 90 mg L^{-1}.

Laboratory experiments were employed to confirm the validity of the predicted optimum conditions. According to

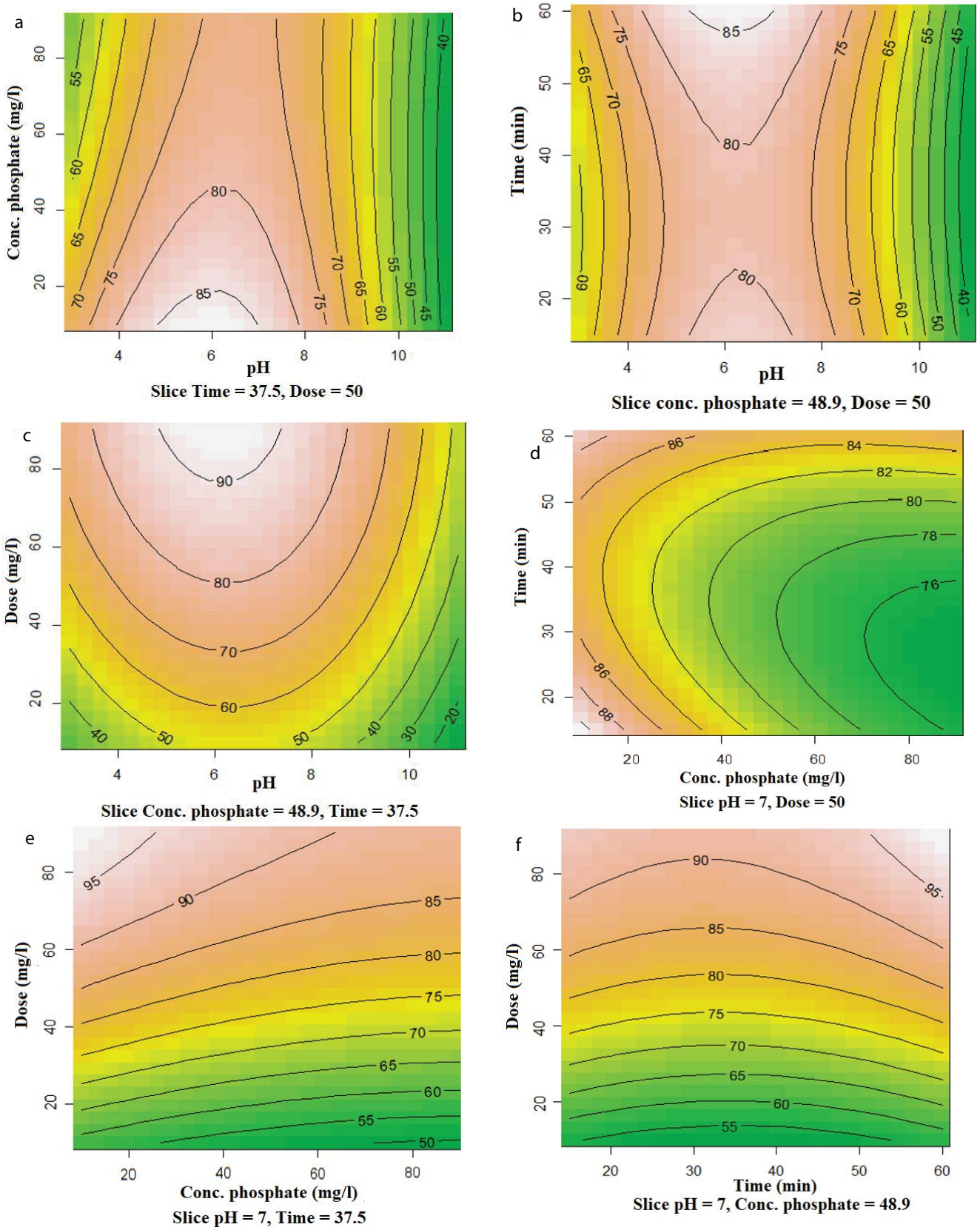

Fig. 3. Contour plot for the effect of conc. phosphate and pH (a), time and pH (b), adsorbent dose and pH (c), time and conc. phosphate (d), adsorbent dose and conc. phosphate (e), and adsorbent dose and time (f).

the results, the experimental data were in good consistency with the above-mentioned optimal conditions.

To obtain the validity of results predicted by the model, additional laboratory experiments were conducted in four replicates. As can be seen in Table 6, experimental data were in good consistency with those predicted by the regression model. In addition, there was another set of experiments shown in Table 6 which was the same as the above-mentioned optimal conditions except for initial pH.

The result showed that the *R*-squared value of the model is very near to the adjusted *R*-squared value. The presence of significant terms in the model demonstrated good agreement between adjusted R^2 (0.97) with predicted R^2 (0.97) which is shown in Fig. 4. This plot indicates the correlation between the actual and predicted efficiency values for the adsorption of phosphate ion by aminated RGC adsorbent, also proves a high linear correlation between them.

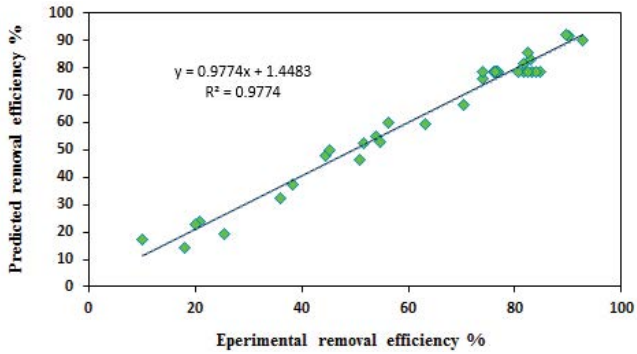

Fig. 4. Correlation of actual and predicted removal efficiency for phosphate.

3.6. Adsorption isotherm studies

The adsorption isotherm models such as Langmuir, Freundlich, and Temkin were employed to explore the adsorption behaviors of the phosphate onto the aminated RGC-derived activated carbon.

In this study, the relationship between the amounts of PO_4^{3-} ions adsorbed at experimental conditions was studied by three isotherm models and equilibrium data were fitted using the correlation coefficient (R^2). The Langmuir model assumes that the adsorbent surface is homogeneous. The adsorbent layers are uniform and monolayer adsorption occurs on a surface with a finite number of adsorption sites and negligible interactions between the molecules [41]. One of the essential characteristics of the Langmuir isotherm modeling is the dimensionless separation factor (R_L) that is described in the following equation:

$$R = \frac{1}{1 + k_1 C_0} \tag{16}$$

where k_1 (L mg^{-1}) is the Langmuir constant and C_0 (mg L^{-1}) is the highest metal ion concentration. The value of R_L is determined the adsorption isotherm: unfavorable ($R_L > 1$), linear ($R_L = 1$), favorable ($0 < R_L < 1$), and irreversible ($R_L = 0$). The Freundlich isotherm model assumes that the adsorbent surface is heterogeneous and the molecules are adsorbed on the surface at different sites and with different adsorption energies. Also, the distribution of energy and interactions between the adsorbent and adsorbate is not uniform. The Temkin isotherm model shows the decrease of the heat of adsorption linearly throughout the adsorption process [42]. The parameters of the Langmuir, Freundlich, and Temkin are presented in Table 7. As the results showed that the maximum adsorption capacity increased with an increase in temperature and reached from 79.5 to 103.5 mg g^{-1}. It was observed that the Freundlich equation is more suitable than Langmuir and Temkin model in the description of the adsorption behavior of PO_4^{3-} on the adsorbent with higher values of correlation coefficients (R^2: 0.99, 0.97, and 0.93, respectively). On the other hand, the value of R_L was in the range of 0.07–0.09; indicating adsorption of phosphate onto aminated RGC adsorbent is favorable at all temperatures. For a favorable adsorption, the value of the Freundlich constant (*n*) should be in the range of 1–10 [43]. The value of the Freundlich constant (*n*) was 2.41, 2.13, and 2.31 for temperatures of 288K, 298K, and 308K, respectively. It indicated that adsorption

Table 6
Experimental and predicted values of the responses at the optimal levels predicted by RSM

pH	Conc. phosphate (mg L^{-1})	Time (min)	Adsorbent dosage (mg L^{-1})	Phosphate removal (%)	
				Predicted	Experimental
5.74	1	32.5	90	100	94.08
7.5	1	32.5	90	94.31	91.48

Table 7
Isotherm parameters for adsorption of phosphate ion onto the aminated RGC adsorbent at different temperatures

Temp. (K)	Langmuir isotherm coefficient				Freundlich isotherm coefficient			Temkin isotherm coefficient		
	q_m (mg g^{-1})	k_L (L mg^{-1})	R^2	R_L	k_f (mg g^{-1})	*n*	R^2	*B* (kJ mol^{-1})	k_t (L mg^{-1})	R^2
288	79.56	1.33	0.9735	0.077	39.04	2.41	0.9868	9.62	0.74	0.9369
298	99.8	1.02	0.9447	0.098	43.73	2.13	0.9948	7.62	0.7	0.9221
308	103.52	1.45	0.9656	0.071	52.47	2.31	0.9948	7.87	0.67	0.9333

was carried out at the favorable condition. The value of K_F at 288K is greater than 308K. The adsorption capacity for aminated RGC adsorbent improves at higher temperatures and heterogeneous adsorption sites at higher temperatures play an important role. Also, the Temkin isotherm is available for heterogeneous adsorption of the aminated RGC adsorbent on a surface. The low value of the equilibrium binding constant (k_t) was related to the weak bonding of the adsorbate onto the medium and the high value of the adsorption heat (B). It also showed the fast sorption of the aminated RGC at the initial stage. According to the results in Table 7, high correlation coefficients (R^2) were found for the Freundlich model compared with the Langmuir and Temkin models that approve a reasonable fit to the data (R^2 of 0.986, 0.994, and 0.994 at 288K, 298K, and 308K temperatures, respectively). Therefore, this indicates that aminated RGC had different adsorption sites and different adsorption energies behavior similar to which that the Freundlich model.

Table 8 shows the results of adsorbent capacity of different adsorbents for phosphate removal and this study. As can see, aminated RGC has a relatively proper capacity for phosphate removal. Therefore, aminated RGC can be suggested as an appropriate and effective adsorbent for phosphate removal from aqueous solution.

3.7. Adsorption kinetic study

Generally, chemical process design is based on the best removal model in the aspect of environmental engineering. Therefore, in order to design chemical processes, it is necessary to carefully evaluate the kinetics of pollutants removal [49]. Hence, the kinetic study of phosphate adsorption onto aminated RGC adsorbent with different contact time-concentration profiles was done with conventional kinetic models including the pseudo-first order, pseudo-second order, Elovich, and intraparticle diffusion. The linear plots of the kinetic models are presented in Fig. 5.

The parameters of the kinetic models are shown in Table 9. q_e (mg g^{-1}) implies the amounts of adsorption at the equilibrium with respect to time t (min). k_1 (min^{-1}) is the adsorption rate constant in the pseudo-first-order model and can be calculated from the slope of the linear plot of log ($q_e - q_t$) versus t. k_2 (g mg^{-1} min^{-1}) is the adsorption rate constants in the pseudo-second-order model that can be obtained from the intercept of the linear plot of t/q_t versus t. The calculated values of q_e from the pseudo-first and pseudo-second-order models are significantly different than the experimental data. The correlation coefficients (R^2) for the pseudo-first-order kinetic model are relatively low (0.79–0.93). Furthermore, rate constants (k_1) of the pseudo-first-order model decreased with increasing initial concentrations which was an obvious disagreement with experimental data that indicated the inefficiency of the model. The correlation coefficients (R^2) for the Elovich kinetic model were relatively low (0.79–0.93). This indicated that the Elovich kinetic model was not suitable for this sorption system. The correlation coefficients (R^2) of the pseudo-second-order kinetic model were relatively high (0.98–0.99). Also, the rate constant of adsorption (k_2) decreased with increasing initial phosphate concentration while the initial adsorption rate (h_0) increased. Thus, R^2 value for all the experimental concentrations close to 1 indicated that the pseudo-second-order model was the most suitable for phosphate adsorption onto aminated RGC adsorbent. Therefore, it could be understood that the rate of adsorption followed the second-order chemisorption. Previous studies showed that the pseudo-second-order model could be used to fit the removal of azo-dyes [50] from the aqueous phase.

The diffusion mechanism and kinetic data were elucidated by the intraparticle diffusion equation, as this model is the rate-limiting step (if the plot of q_t versus $t^{1/2}$ is a straight line). The model is represented as:

$$q_t = k_d t^{1/2} + I \tag{17}$$

where k_d is the intraparticle diffusion rate constant (mg g^{-1} min$^{-1/2}$) and I is the intercept. I indicates the thickness of boundary layer [51]. The Adj.R^2 for the intraparticle diffusion model was between 0.90 and 0.95. According to this model, if the plot of q_t versus $t^{1/2}$ is linear, and the lines pass through the origin, intraparticle diffusion will involve in the adsorption process. Also, multilinear plots involve various steps, as a result, two or more steps influence the adsorption process. Fig. 5(d) shows the intraparticle diffusion plots for the different concentrations of phosphate adsorption onto aminated RGC adsorbent. As it is shown in Fig. 5(d), the plots did not pass through the origin, indicating that all the plots had the same general feature and were multilinear. Furthermore, there is some degree of boundary layer control effects that shows the external diffusion and the intraparticle diffusion was two steps of the sorption process. In the study, the initial curved portion was followed

Table 8
Comparison of adsorption capacity between the results of this study and other researches

Adsorbent	Adsorption capacity (mg g^{-1})	Reference
This study	99.8	–
Pectin based quaternary amino anion exchanger Graphene	31.07	[20]
	89.37	[44]
Wheat straw based anion exchanger	45.7	[45]
Agricultural by-products anion exchange resins	52.4	[46]
Acrylonitrile/divinylbenzene/vinylbenzyl chloride skeleton resin	183.18	[47]
Cubic zeolitic imidazolate framework-8	38.22	[48]

Table 9
Kinetic parameters for adsorption of phosphate ion onto the aminated RGC adsorbent at different initial concentrations

C_0 (mg L^{-1})	$q_{e,exp.}$ (mg L^{-1})	Pseudo-first order			Pseudo-second order			Elovich			Intra-particle diffusion		
		$q_{e,cal.}$ (mg L^{-1})	k_1 (min^{-1})	R^2	$q_{e,cal.}$ (mg g^{-1})	k_2 (g mg^{-1} min^{-1})	h_0 (mg g^{-1} min^{-1})	R^2	A (mg g^{-1} min^{-1})	B (g mg^{-1})	R^2	k_d (mg g^{-1} min$^{-1/2}$)	I (mg g^{-1})	R^2
10	1.001	0.48	0.079	0.7937	11.53	2.95	3.93	0.9989	108.45	125	0.7937	0.234	8.77	0.9057
50	3.4	2.96	0.065	0.9393	53.81	0.18	5.29	0.9949	222.24	10.5	0.9393	3.45	20.52	0.9593
90	4.622	3.38	0.033	0.8867	80.85	0.1	6.44	0.9886	142.94	6.5	0.8867	5.42	26.36	0.9439

by a gradual adsorption, therefore, the faster adsorption stage may be considered as an external surface adsorption and the intraparticle diffusion was rate-controlled. The plateau portion of the curve was related to the final equilibrium stage and intraparticle diffusion started to slow down because of the extremely low adsorbate concentrations in the solution [52]. Higher values of k_d (indicates rapid transfer) and I confirmed intraparticle diffusion as the dominant mechanism for the adsorption of phosphate onto aminated RGC adsorbent. This further showed that the intraparticle diffusion might be the dominant step for the adsorption and the intraparticle diffusion was not the only rate-limiting step [53].

3.8. Thermodynamic study

The thermodynamic study was required for determining the energy of system and mechanism of adsorption. The results of thermodynamic study are shown in Table 10.

The negative value of enthalpy showed that the adsorption reaction is spontaneity. In addition, the negative values of the enthalpy presented that the nature of adsorption reaction is exothermic [54]. The mechanism of adsorption could be determined according to the free energy. The value of free energy between −20 and 0 kJ mol^{-1} is the physio-sorption, −20 to –80 kJ mol^{-1} is the physio-chemisorption, and −80 to −400 kJ mol^{-1} is chemisorption. Therefore, the value of free energy showed that the mechanism of phosphate adsorption onto aminated RGC was physio-chemisorption.

3.9. Regeneration tests

Desorption and regeneration tests were carried out to determine the desorption efficiencies and reusability of the aminated RGC. The results of phosphate desorption efficiency are shown in Table 11. According to the results, the

Table 10
Thermodynamic parameters of phosphate adsorption onto aminated RGC

Temperature (°K)	$\Delta G°$ (kJ mol^{-1})	$\Delta H°$ (kJ mol^{-1})	$\Delta S°$ (J mol^{-1} K)
288	–25.93		
298	–26.49	–9.71	56.32
308	–27.05		

Table 11
Regeneration of aminated RGC for adsoprtion of phosphate

Regeneration cycles	Adsorption capacity (mg g^{-1})	Efficiency of desorption (%)
Original adsorbent	97.44	97.52
1	95.25	95.14
2	93.84	93.75
3	90.72	91.52
4	87.87	87.46
5	83.59	84.05

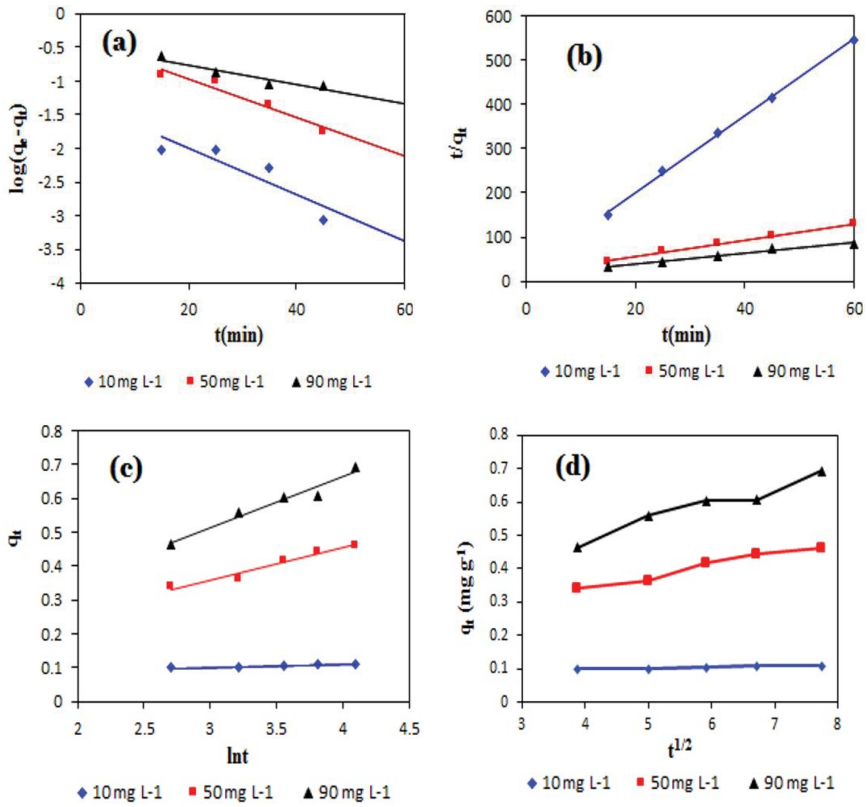

Fig. 5. Pseudo-first order (a), pseudo-second order (b), Elovich (c), intraparticle diffusion and (d) kinetic models for the adsorption of phosphate onto aminated RGC (temperature = 288 K, pH = 3, contact time = 15–60 min, and adsorbent dose = 90 mg L^{-1}).

adsorption capacity of phosphate onto the aminated RGC had a negligible drop during adsorption–regeneration cycles. In addition, HCl (0.1 mol L^{-1}) could be considered as the eluent with solution/solid ratio of 50:1 for regenerating the aminated RGC after the adsorption of phosphate.

4. Conclusions

In this study, the adsorption of phosphate onto aminated RGC adsorbent at the solid/aqueous interface was investigated. The quadratic equations developed for this study showing good correlation between experimental and model predicted values. The results such as *p*-value (2.2×10^{-16}), higher *F*-value (116.6), R^2 (multiple *R*-squared: 0.9774, adjusted *R*-squared: 0.97), insignificant lack of fit (0.167) indicated that the reduced full second-order model was highly significant for phosphate removal by aminated RGC. Being close to the *R*-squared value of the model to the adjusted *R*-squared value indicated that the quadratic regression related to the reduced full second-order model could be used for prediction and optimization. The maximum removal efficiency of phosphate was 92.76 which was obtained at optimum operating conditions, pH = 3, initial phosphate concentrations (10 mg L^{-1}), contact time (60 min), and adsorbent dose (90 mg L^{-1})). The maximum removal efficiency was estimated to be 100% using regression coefficients obtained from the model and Solver "Add-ins." The predicted optimal conditions by the Solver "Add-ins" were obtained at pH; 5.74, the initial phosphate concentration of 10 mg L^{-1}, contact time of 32.5 min, and adsorbent dosage of 90 mg L^{-1}. The surface characterization of aminated RGC such as XRF, FT-IR, and FESEM indicated that the surface of the aminated RGC showed irregular texture with finer particles size, rough surface, and the leaf-like edges. The EDS spectra of the aminated RGC adsorbent showed weight percentage of O, C, Ca, Mg, Fe, Al, and P after phosphate uptake. The functional groups involved in adsorption of phosphate onto aminated RGC as follow C=O, C–H, C–O, and C–N. The relationship between the amounts of PO_4^{3-} ions adsorbed onto aminated RGC adsorbent was described by isotherm and kinetic models. The results show that the adsorption data fitted well the Freundlich isotherm compared with the Langmuir and Temkin models. High predicted R^2 values were obtained for the pseudo-second-order kinetic model. Therefore, the adsorption kinetics was best fitted with the pseudo-second-order kinetic model to describe the experimental data. Furthermore, the calculation of intraparticle diffusion model showed that this model was the dominant mechanism for the adsorption but it was not the only rate-limiting step.

Acknowledgments

The author would like to appreciate the financial support of NIMAD on this research project as Code No. 963259 by the Ministry of Health, Iran. In addition, the author would like to thanks the staff of the water and wastewater chemistry, School of Public Health Tehran University of Medical Sciences, Tehran, Iran.

References

[1] M. Khazaei, R. Nabizadeh, A.H. Mahvi, H. Izanloo, R. Ansari Tadi, F. Gharagazloo, Nitrogen and phosphorous removal from aerated lagoon effluent using horizontal roughing filter (HRF), Desal. Wat. Treat., 57 (2016) 5425–5434.

[2] H. Gharibi, A. Mahvi, M. Chehrazi, R. Sheikhi, S. Hosseini, Phosphorous removal from wastewater effluent using electro-coagulation by aluminum and iron plates, Anal. Bioanal. Chem., 2 (2010) 165–177.

[3] A. Drenkova-Tuhtan, M. Schneider, M. Franzreb, C. Meyer, C. Gellermann, G. Sextl, K. Mandel, H. Steinmetz, Pilot-scale removal and recovery of dissolved phosphate from secondary wastewater effluents with reusable ZnFeZr adsorbent@ Fe_3O_4/SiO_2 particles with magnetic harvesting, Water Res., 109 (2017) 77–87.

[4] F. Fu, D.D. Dionysiou, H. Liu, The use of zero-valent iron for groundwater remediation and wastewater treatment: a review, J. Hazard. Mater., 267 (2014) 194–205.

[5] N. Sleiman, V. Deluchat, M. Wazne, M. Mallet, A. Courtin-Nomade, V. Kazpard, M. Baudu, Phosphate removal from aqueous solutions using zero valent iron (ZVI): influence of solution composition and ZVI aging, Colloids Surf., A, 514 (2017) 1–10.

[6] D.J. Conley, Ecology: save the Baltic Sea, Nature, 486 (2012) 463–464.

[7] S. Faridmarandi, G.M. Naja, Phosphorus and water budgets in an agricultural basin, Environ. Sci. Technol., 48 (2014) 8481–8490.

[8] D. Chen, P. Szostak, Z. Wei, R. Xiao, Reduction of orthophosphates loss in agricultural soil by nano calcium sulfate, Sci. Total Environ., 539 (2016) 381–387.

[9] A.T. Tran, Y. Zhang, D. De Corte, J.-B. Hannes, W. Ye, P. Mondal, N. Jullok, B. Meesschaert, L. Pinoy, B. Van der Bruggen, P-recovery as calcium phosphate from wastewater using an integrated selectrodialysis/crystallization process, J. Cleaner Prod., 77 (2014) 140–151.

[10] Y. Zhang, E. Desmidt, A. Van Looveren, L. Pinoy, B. Meesschaert, B. Van der Bruggen, Phosphate separation and recovery from wastewater by novel electrodialysis, Environ. Sci. Technol., 47 (2013) 5888–5895.

[11] L. Rafati, R. Nabizadeh, A.H. Mahvi, M.H. Dehghani, Removal of phosphate from aqueous solutions by iron nano-particle resin Lewatit (FO36), Korean J. Chem. Eng., 29 (2012) 473–477.

[12] N. Yousefi, A. Fatehizedeh, K. Ghadiri, N. Mirzaei, S.D. Ashrafi, A.H. Mahvi, Application of nanofilter in removal of phosphate, fluoride and nitrite from groundwater, Desal. Wat. Treat., 57 (2016) 11782–11788.

[13] A.H. Mahvi, S.J.A.-D. Ebrahimi, A. Mesdaghinia, H. Gharibi, M.H. Sowlat, Performance evaluation of a continuous bipolar electrocoagulation/electrooxidation–electroflotation (ECEO–EF) reactor designed for simultaneous removal of ammonia and phosphate from wastewater effluent, J. Hazard. Mater., 192 (2011) 1267–1274.

[14] A.J. Erickson, J.S. Gulliver, P.T. Weiss, Capturing phosphates with iron enhanced sand filtration, Water Res., 46 (2012) 3032–3042.

[15] A. Rajeswari, A. Amalraj, A. Pius, Removal of phosphate using chitosan-polymer composites, J. Environ. Chem. Eng., 3 (2015) 2331–2341.

[16] P. Wilfert, P.S. Kumar, L. Korving, G.-J. Witkamp, M.C. van Loosdrecht, The relevance of phosphorus and iron chemistry to the recovery of phosphorus from wastewater: a review, Environ. Sci. Technol., 49 (2015) 9400–9414.

[17] J. Lalley, C. Han, G.R. Mohan, D.D. Dionysiou, T.F. Speth, J. Garland, M.N. Nadagouda, Phosphate removal using modified Bayoxide® E33 adsorption media, Environ. Sci.: Water Res. Technol., 1 (2015) 96–107.

[18] J. Keeley, A.D. Smith, S.J. Judd, P. Jarvis, Acidified and ultrafiltered recovered coagulants from water treatment works sludge for removal of phosphorus from wastewater, Water Res., 88 (2016) 380–388.

[19] S.K. Ghadiri, S. Nasseri, R. Nabizadeh, M. Khoobi, S. Nazmara, A.H. Mahvi, Adsorption of nitrate onto anionic bio-graphene nanosheet from aqueous solutions: isotherm and kinetic study, J. Mol. Liq., 242 (2017) 1111–1117.

[20] M. Naushad, G. Sharma, A. Kumar, S. Sharma, A.A. Ghfar, A. Bhatnagar, F.J. Stadler, M.R. Khan, Efficient removal of toxic phosphate anions from aqueous environment using pectin based quaternary amino anion exchanger, Int. J. Biol. Macromol., 106 (2018) 1–10.

[21] Y. Wang, R. Yang, Y. Wei, Z. Zhao, M. Li, Preparation of novel pigskin-derived carbon sheets and their low-temperature activation-induced high capacitive performance, RSC Adv., 4 (2014) 45318–45324.

[22] H. Muramatsu, Y.A. Kim, K.S. Yang, R. Cruz-Silva, I. Toda, T. Yamada, M. Terrones, M. Endo, T. Hayashi, H. Saitoh, Rice husk-derived graphene with nano-sized domains and clean edges, Small, 10 (2014) 2766–2770.

[23] G. Ramesha, A.V. Kumara, H. Muralidhara, S. Sampath, Graphene and graphene oxide as effective adsorbents toward anionic and cationic dyes, J. Colloid Interface Sci., 361 (2011) 270–277.

[24] S. Zhang, Y. Shao, J. Liu, I.A. Aksay, Y. Lin, Graphene–polypyrrole nanocomposite as a highly efficient and low cost electrically switched ion exchanger for removing ClO_4–from wastewater, ACS Appl. Mater. Interfaces, 3 (2011) 3633–3637.

[25] Y. Li, P. Zhang, Q. Du, X. Peng, T. Liu, Z. Wang, Y. Xia, W. Zhang, K. Wang, H. Zhu, Adsorption of fluoride from aqueous solution by graphene, J. Colloid Interface Sci., 363 (2011) 348–354.

[26] S. Wang, H. Sun, H.-M. Ang, M. Tadé, Adsorptive remediation of environmental pollutants using novel graphene-based nanomaterials, J. Chem. Eng., 226 (2013) 336–347.

[27] A. Mahvi, Application of agricultural fibers in pollution removal from aqueous solution, IJEST, 5 (2008) 275–285.

[28] M.A. Zazouli, A.H. Mahvi, S. Dobaradaran, M. Barafrashtehpour, Y. Mahdavi, D. Balarak, Adsorption of fluoride from aqueous solution by modified Azolla filiculoides, Fluoride, 47 (2014) 349–358.

[29] A. Mahvi, F. Gholami, S. Nazmara, Cadmium biosorption from wastewater by Ulmus leaves and their ash, Eur. J. Sci. Res., 23 (2008) 197–203.

[30] A. Maleki, A.H. Mahvi, M.A. Zazouli, H. Izanloo, A.H. Barati, Aqueous cadmium removal by adsorption on barley hull and barley hull ash, Asian J. Chem., 23 (2011) 1373.

[31] Z.A. ALOthman, M. Naushad, R. Ali, Kinetic, equilibrium isotherm and thermodynamic studies of Cr(VI) adsorption onto low-cost adsorbent developed from peanut shell activated with phosphoric acid, Environ. Sci. Pollut. Res., 20 (2013) 3351–3365.

[32] N. Yousefi, R. Nabizadeh, S. Nasseri, M. Khoobi, S. Nazmara, A.H. Mahvi, Decolorization of direct blue 71 solutions using tannic acid/polysulfone thin film nanofiltration composite membrane; preparation, optimization and characterization of anti-fouling, Korean J. Chem. Eng., 34 (2017) 2342–2353.

[33] N. Yousefi, R. Nabizadeh, S. Nasseri, M. Khoobi, S. Nazmara, A.H. Mahvi, Optimization of the synthesis and operational parameters for NOM removal with response surface methodology during nano-composite membrane filtration, Water Sci. Technol., 77 (2018) 1558–1569.

[34] M. Khazaei, S. Nasseri, M.R. Ganjali, M. Khoobi, R. Nabizadeh, A.H. Mahvi, E. Gholibegloo, S. Nazmara, Modeling mercury (II) removal at ultra-low levels from aqueous solution using graphene oxide functionalized with magnetic nanoparticles: optimization, kinetics, and isotherm studies, Desal. Wat. Treat., 83 (2017) 144–158.

[35] S. Ghadiri, R. Nabizadeh, A. Mahvi, S. Nasseri, A. Mesdaghinia, S. Talebi, Potential of granulated modified nanozeolites Y for MTBE removal from aqueous solutions: kinetic and isotherm studies, Pol. J. Chem. Technol., 14 (2012) 1–8.

[36] M. Naushad, T. Ahamad, B.M. Al-Maswari, A.A. Alqadami, S.M. Alshehri, Nickel ferrite bearing nitrogen-doped mesoporous carbon as efficient adsorbent for the removal of highly toxic metal ion from aqueous medium, Chem. Eng. J., 330 (2017) 1351–1360.

[37] A.A. Alqadami, M. Naushad, Z.A. Alothman, A.A. Ghfar, Novel metal–organic framework (MOF) based composite material for the sequestration of U (VI) and Th (IV) metal ions

from aqueous environment, ACS Appl. Mater. Interfaces, 9 (2017) 36026–36037.
[38] E.-R. Kenawy, A.A. Ghfar, M. Naushad, Z.A. ALOthman, M.A. Habila, A.B. Albadarin, Efficient removal of Co (II) metal ion from aqueous solution using cost-effective oxidized activated carbon: kinetic and isotherm studies, Desal. Wat. Treat., 70 (2017) 220–226.
[39] J. Wu, D. Yu, H. Sun, Y. Zhang, W. Zhang, F. Meng, X. Du, Optimizing the extraction of anti-tumor alkaloids from the stem of *Berberis amurensis* by response surface methodology, Ind. Crops Prod., 69 (2015) 68–75.
[40] A. Rahmani, J. Nouri, S. Kamal Ghadiri, A.H. Mahvi, M.R. Zare, Adsorption of fluoride from water by Al^{3+} and Fe^{3+} pretreated natural Iranian zeolites, Int. J. Environ. Res., 4 (2010) 607–614.
[41] M.A. Fard, B. Barkdoll, Using recyclable magnetic carbon nanotube to remove micropollutants from aqueous solutions, J. Mol. Liq., 249 (2018) 193–202.
[42] P. Wu, S. Li, L. Ju, N. Zhu, J. Wu, P. Li, Z. Dang, Mechanism of the reduction of hexavalent chromium by organo-montmorillonite supported iron nanoparticles, J. Hazard. Mater., 219 (2012) 283–288.
[43] G. Moussavi, R. Khosravi, Removal of cyanide from wastewater by adsorption onto pistachio hull wastes: parametric experiments, kinetics and equilibrium analysis, J. Hazard. Mater., 183 (2010) 724–730.
[44] S. Vasudevan, J. Lakshmi, The adsorption of phosphate by graphene from aqueous solution, RSC Adv., 2 (2012) 5234–5242.
[45] X. Xu, B.-Y. Gao, Q.-Y. Yue, Q.-Q. Zhong, Preparation of agricultural by-product based anion exchanger and its utilization for nitrate and phosphate removal, Bioresour. Technol., 101 (2010) 8558–8564.
[46] X. Xu, B.-Y. Gao, Q.-Y. Yue, Q.-Q. Zhong, Q. Li, Preparation of new types of anion exchange resins from agricultural by-products and their utilization in the removal of various toxic anions from solutions, Chem. Eng. J., 167 (2011) 104–111.
[47] A. Sowmya, S. Meenakshi, A novel quaternized resin with acrylonitrile/divinylbenzene/vinylbenzyl chloride skeleton for the removal of nitrate and phosphate, Chem. Eng. J., 257 (2014) 45–55.
[48] M. Shams, M.H. Dehghani, R. Nabizadeh, A. Mesdaghinia, M. Alimohammadi, A.A. Najafpoor, Adsorption of phosphorus from aqueous solution by cubic zeolitic imidazolate framework-8: modeling, mechanical agitation versus sonication, J. Mol. Liq., 224 (2016) 151–157.
[49] S. Abuzerr, M. Darwish, A. Mohammadi, S.S. Hosseini, A.H. Mahvi, Enhancement of Reactive Red 198 dye photo catalytic degradation using physical mixtures of ZnO-graphene nanocomposite and TiO_2 nanoparticles: an optimized study by response surface methodology, Desal. Wat. Treat., doi:10.5004/dwt.2018.23259.
[50] W. Konicki, M. Aleksandrzak, D. Moszyński, E. Mijowska, Adsorption of anionic azo-dyes from aqueous solutions onto graphene oxide: equilibrium, kinetic and thermodynamic studies, J. Colloid Interface Sci., 496 (2017) 188–200.
[51] K. Vilcinskas, J. Zlopasa, K. Jansen, F.M. Mulder, S.J. Picken, G.J. Koper, Water sorption and diffusion in (reduced) graphene oxide-alginate biopolymer nanocomposites, Macromol. Mater. Eng., 301 (2016) 1049–1063.
[52] S. Yu, X. Wang, Y. Ai, X. Tan, T. Hayat, W. Hu, X. Wang, Experimental and theoretical studies on competitive adsorption of aromatic compounds on reduced graphene oxides, J. Mater. Chem., 4 (2016) 5654–5662.
[53] Y. Han, W. Li, J. Zhang, H. Meng, Y. Xu, X. Zhang, Adsorption behavior of Rhodamine B on nanoporous polymers, RSC Adv., 5 (2015) 104915–104922.
[54] Z.H. Mousavi, A. Hosseinifar, V. Jahed, Studies of adsorption thermodynamics and kinetics of Cr (III) and Ni (II) removal by polyacrylamide, J. Serb. Chem. Soc., 77 (2012) 393–405.